IOP Publishing Journal of Physics: Condensed Matter
J. Phys.: Condens. Matter **32** (2020) 285403 (7pp) https://doi.org/10.1088/1361-648X/ab808e

# Sub-THz Raman response in $BaTiO_3$ and link with structural phase transition

**Marc D Fontana[1,2], Ninel Kokanyan[1,2] and Thomas H Kauffmann[1,2]**

[1] Université de Lorraine, CenraleSupélec, LMOPS, F-57000 Metz, France
[2] Laboratoire Matériaux Optiques, Photonique et Systèmes, CentraleSupélec, Université Paris-Saclay, Metz, 57070, Metz, France

E-mail: thomas.kauffmann@univ-lorraine.fr

Received 3 December 2019, revised 2 March 2020
Accepted for publication 17 March 2020
Published 17 April 2020

**Abstract**

The THz and sub-THz polarized Raman response was measured in tetragonal and cubic phases of single domain $BaTiO_3$ crystal. A large peak was detected at very low wavenumber, within a scattering geometry in which all phonon lines are Raman inactive. It lies below 700 GHz in the whole temperature range of the tetragonal phase, and is clearly distinct from the soft phonon band. This peak has relaxational behavior with a slowing down on approaching the phase transition from above and from below.

Keywords: ferroelectrics, phase transitions, $BaTiO_3$, Raman spectroscopy, phonon, relaxation, order–disorder

(Some figures may appear in colour only in the online journal)

## 1. Introduction

Barium titanate $BaTiO_3$ (BTO) is one of the most extensively studied ferroelectric materials and is of practical importance for capacitors, electrocaloric and pyroelectric devices. The understanding and control of its dielectric properties is therefore a major issue. BTO attracted also much attention for fundamental research since it undergoes the successive cubic–tetragonal–orthorhombic–rhombohedral (C–T–O–R) phases on cooling [1, 2]. BTO is often quoted as a textbook substance to study the mechanism of structural phase transitions (SPT).

The nature, displacive or order–disorder (O–D), of the C–T SPT has been the subject of many investigations and controversies. The displacive model was supported by the detection of a soft phonon on approaching the C–T transition, as evidenced by means of infrared (IR) [3] hyper-Raman (HR) [4] and Raman spectroscopy [5].

The O–D behavior was suggested a long time ago from the detection of strong diffuse x-ray scattering [6] and confirmed by more recent x-ray absorption fine structure investigations [7]. The O–D picture is related to off-center Ti ions along diagonal cubic directions. Relaxational (hopping) motion is expected between these equivalent sites. This approach was corroborated by pseudo Jahn–Teller model inducing local eight-minima adiabatic potential energy surface [8]. This description was also supported by Brillouin scattering measurements showing a strong central peak besides a softening of longitudinal acoustic phonon in the C phase [9]. It should be underlined that the distinction between O–D and displacive pictures is generally not simple. Thus, by means of new highly resolved x-ray measurements, the diffuse scattering was recently analyzed in terms of overdamped anharmonic soft phonon branch within the displacive picture [10].

The coexistence of both displacive and O–D processes was predicted by *ab initio* calculations [11, 12], or was indirectly derived from the discrepancy in dielectric permittivity between direct data and calculations via Lyddane–Sachs–Teller relationship [13–15].

Therefore the possibility of existence of two critical degrees of freedom is now admitted but the direct observation of the relaxational mode by optical spectroscopy gives contradictory results [16, 17]. A central peak was observed by quasielastic scattering (QES) and attributed to a relaxation mode [18, 19] but femto-second time resolved spectroscopy data ruled out this possibility [20].

More recently, the dielectric response within THz range was investigated by means of IR and THz spectroscopy [13, 21, 22] and displayed the existence of two modes in T and C phases. Soft phonon and relaxation peak were

 

simultaneously detected in these studies but the data analysis needed a large of number of parameters, limiting their reliability. The results were in contradiction with earlier data [3, 4, 20] and gave rise to a large bare relaxation rate (above 100 $cm^{-1}$). Therefore the origin and characteristics of this second mode remains unclear and the question about one or two modes persists. In principle the Rayleigh line and the very high damping of the soft phonon [5] make difficult the detection by Raman scattering of the relaxational mode which should be located at small wavenumber. Therefore we have undertaken new Raman measurements on BTO single crystals in THz and sub-THz range, using an appropriate Raman set up. In addition, we considered scattering geometries which discard the soft phonon peak and were up to now never explored. We used configurations providing either longitudinal optical $A_1$(LO) lines, or the 'extinction spectrum', for which all phonons are Raman inactive. The last configuration clearly highlights a sub-THz scattered signal with a critical behavior on approaching the SPT while the first geometry allows to detect the phase transition without any ambiguity. Measurements were carried out as function of temperature in the T and C phases and data were analyzed and discussed in the framework of the long-standing controversy about the SPT mechanism.

## 2. Raman (basics and experiments)

Raman measurements have been carried out on single crystals of BTO as function of temperature from 300 up to 450 K, i.e. in the T and C phases. It is reminded that in the C phase the first-order Raman scattering is in principle forbidden and only second-order bands are detected [23].

In the T phase ($C_{4v}$ or 4 mm) the optical phonons at the center of the Brillouin zone are written into irreducible representations as:

$$T_\Gamma = 3A_1(Z) + 4E^{(2)}(X, Y) + B_1 \quad (1)$$

where the letter in brackets corresponds to the direction of dipole moment associated with the phonon. $A_1$ and $E$ modes are Raman and IR active while $B_1$ is only Raman active. No dipole is associated with this last mode. It is reminded [22, 23] that the $A_1$ modes correspond to ionic vibrations along the ferroelectric (FE) $c$ axis, while the $E$ phonons involve motions in the ($ab$) plane normal to $c$.

The Raman tensors of modes in T phase are written as:

$$A_1(Z) = \begin{pmatrix} a & 0 & 0 \\ 0 & a & 0 \\ 0 & 0 & b \end{pmatrix} B_1 = \begin{pmatrix} c & 0 & 0 \\ 0 & c & 0 \\ 0 & 0 & 0 \end{pmatrix}$$

$$E(X) = \begin{pmatrix} 0 & 0 & d \\ 0 & 0 & 0 \\ d & 0 & 0 \end{pmatrix} E(Y) = \begin{pmatrix} 0 & 0 & 0 \\ 0 & 0 & d \\ 0 & d & 0 \end{pmatrix}$$

According to Raman selection rules, transverse optical $E$(TO) modes including the usual soft phonon, and $A_1$(TO) modes are expected in backscattering X(YZ)$\bar{X}$ and X(ZZ)$\bar{X}$ configurations respectively. The $A_1$(LO) + $B_1$ modes can be detected within the Z(XX)$\bar{Z}$ configuration. It is to be underlined that the (XY) component is null in all Raman tensors. Therefore no first order Raman line is expected in the Z(XY)$\bar{Z}$ configuration, which consequently will be called the 'extinction spectrum'.

High quality BTO crystals grown by top seeded solution growth were provided by Rytz at FEE GmbH. A mainly single domain sample was obtained on cooling just above the Curie temperature by the application of DC electric field. Raman measurements were performed on the spectroscopy platform of the LMOPS. Spectra were recorded in backscattering and various polarized configurations using a confocal Raman microscope LabRAM HR Evolution (Horiba) with an exciting line of 532 nm. Spectra were recorded as function of temperature ranging from 300 to 460 K using a HFS600E stage (*Linkam*) to control the temperature of the crystal within 1 K. The Raman system leads to a spectral resolution of 1 $cm^{-1}$ using a 1800 grooves per millimeter grating and is equipped with an ultra-low frequency (ULF) module. The ULF module consists of three Notch filters in a row rejecting the laser line centered at 0 $cm^{-1}$ and wavenumbers down to $\pm$ 5 $cm^{-1}$.

## 3. Results

### 3.1. Spectra at room temperature

Firstly, we briefly compare in figure 1 the spectra recorded in four main configurations and we explain our choice of focusing our attention on two of them. The scattering geometries giving rise to the detection of soft or hard components of the FE mode were usually considered [5, 23, 25, 26].

The X(YZ)$\bar{X}$ spectrum, giving rise to the detection of $E$(TO) phonons, is the most important since it includes the soft phonon and possibly the central peak that are both claimed to drive the SPT from T to O phase. They are related to a wide and intense scattering detected in low wavenumber. In fact, this signal is difficult to separate into between phonon and relaxation responses, which is the subject of many contradictions and controversies in the literature [16, 18, 19].

The spectrum recorded in the X(ZZ)$\bar{X}$ configuration has a less interest than the $E$ spectrum, although it contains the vibrational response along the FE axis. The $A_1$(TO) spectrum strongly differs in its profile and intensity from the $E$ spectrum, reflecting the large anisotropy of the dielectric properties of BTO, regarding the FE axis, or the plane normal to it. The $A_1$(TO) spectrum displays both second- and first-order bands, in particular the most intense peak lying around 280 $cm^{-1}$, which is the hard component of the cubic soft mode that stiffens at the C–T SPT. Furthermore, the $A_1$(TO) phonons are highly anharmonic, as shown by their thermal behavior [23].

We also present in figure 1 the results obtained in other configurations that have not been explored yet. They provide a complementary view to $E$(TO) and $A_1$(TO) spectra, but they also give information on the C–T SPT, which cannot be obtained—or with difficulty—by the others. At first, we consider the Z(XX)Z spectrum, corresponding to the activation of $3A_1$(LO) + $B_1$ modes. These 4 first-order lines are detected and can be unambiguously distinguished from the

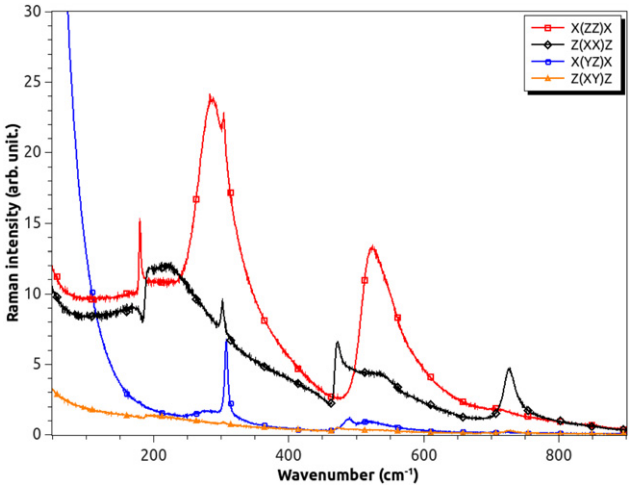


**Figure 1.** Polarized Raman spectra recorded at room temperature on a single-domain $BaTiO_3$ crystal.

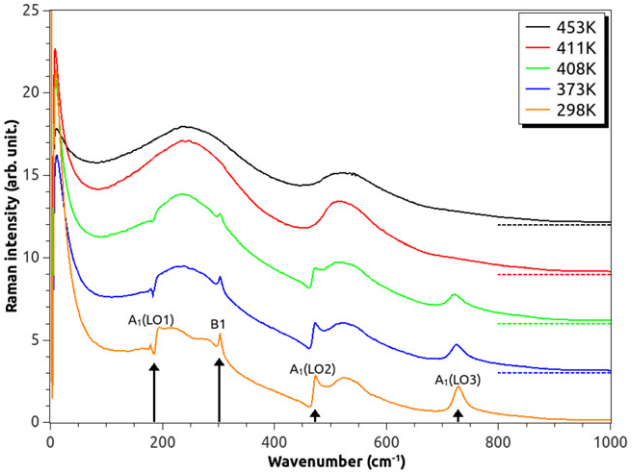


**Figure 2.** $Z(XX)\bar{Z}$ Raman spectrum recorded at different temperatures on a single domain $BaTiO_3$ crystal. The arrows indicate the position of the first-order lines $A_1$(LO) and $B_1$. The dashed line corresponds to zero intensity line for each temperature.

second order bands, without any treatment, unlike the (ZZ) $A_1$(TO) spectrum [23].

At last, we focus attention to the 'extinction spectrum'. Indeed, as it will be used in detail below, the very low-frequency (VLF) signal and thus the QES or any additional degree of freedom lying at low-frequency, if it does exist, could be clearly detected in the XY spectrum, since according to Raman selection rules, no phonon is active. The VLF signal in the XY spectrum cannot be, even partly, hidden by first or second order scattering, contrary to the cases of (XZ) E(TO) and (ZZ) $A_1$(TO) spectra. In addition, the XY extinction spectrum is useful for indirectly check the single domain character and the optical quality of the sample as well as the correct orientation of the crystal axes with respect to the polarizers. This is of major importance for achieving a reliable analysis of polarized Raman spectra. It is indeed well known that a small disorientation can cause a detection of lines due to a leakage of modes of another symmetry, rendering difficult the interpretation of spectra.

As seen in figure 1, no line occurs in the 'extinction spectrum' XY in accordance with what is expected. The scattered intensity at 200 $cm^{-1}$ is more than 10 times lower than this of the XX spectrum recorded in the same conditions. By contrast, the intensity at low frequency is not negligible even if it is smaller than that in the XX and ZZ spectra.

It should be pointed that all 4 spectra recorded at room temperature (and shown in figure 1) strictly respect the Raman selection rules, which reinforces the reliability of the analysis below.

### 3.2. XX $A_1$(LO) spectra

The XX spectrum shown in figure 2 exhibits narrow lines corresponding to expected $3A_1$(LO) + $B_1$ lines and wide bands attributed to second order scattering process. The first-order phonons occur at 185 $cm^{-1}$ [$A_1$(LO1)] (as a Fano resonance), 302 $cm^{-1}$ ($B_1$), 473 $cm^{-1}$ [$A_1$(LO2)] and 728 $cm^{-1}$ [$A_1$(LO3)].

With increasing temperature all the first-order lines are less and less pronounced, reflecting an intensity decrease while

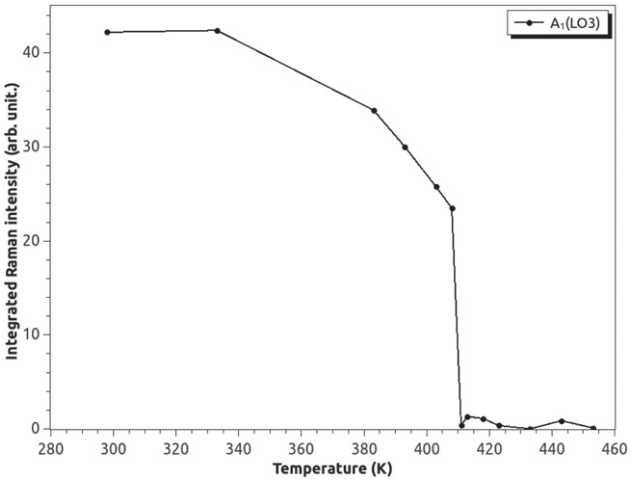


**Figure 3.** Temperature dependence of the integrated intensity $J$ of the $A_1$(LO3) peak in single-domain $BaTiO_3$ crystal. $J$ is calculated by integration after subtraction of a linear baseline. Above $T_c$ the non-zero value of the intensity can be related to pre-transitional features extensively reported in literature [27].

the second-order bands simultaneously become stronger. The opposite thermal behavior of narrow and broad features confirms their respective first- and second-order scattering origin. Above 408 K the whole spectrum displays a large change in profile with the clear disappearance of first-order lines and an abrupt increase of the intensity of the wide bands that remain in the same positions.

These both observations are fully consistent with the first-order character of the transition during the heating from T to C phase, in which the first-order phonons are Raman inactive.

This assertion is corroborated in figure 3 by the plot as a function of the temperature of the integrated intensity $J$ of the peak $A_1$(LO3), that abruptly goes to zero at 409 K, taken hereafter as the C–T transition temperature $T_c$. Note that for the peaks $B_1$ and $A_1$(LO2) the decrease of these lines is

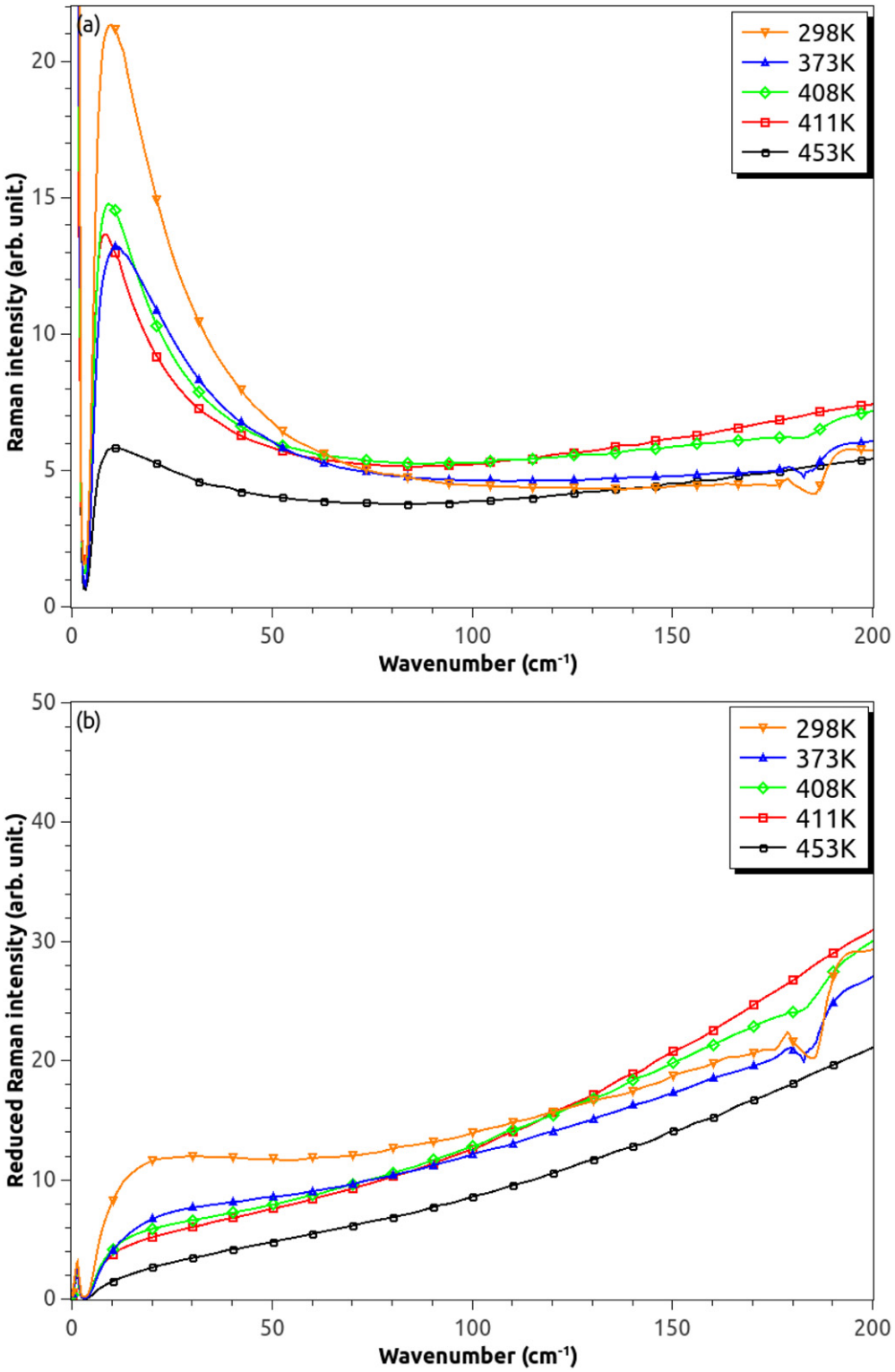


**Figure 4.** Low-frequency Z(XX)$\bar{Z}$ Raman spectrum recorded at different temperatures on single $BaTiO_3$ crystal: (a) raw data, (b) corrected data according to equation (2).

partly masked by the increasing and superimposed wide bands, which makes any calculation of the integrated intensity more difficult.

We can observe that the temperature dependence of $J$ is rather similar to this of the spontaneous polarization [1]. In fact, the phonons $A_1$ correspond to vibrations along the distorted $c$ axis occurring at $T_c$.

We turn now to the behavior of the spectrum at lower frequency. As seen in figure 4(a), a strong and wide signal is detected at VLF, while no first-order phonon is expected in this

range. Moreover, the VLF intensity shows a strong dependence on temperature.

Hereafter, for in-depth analysis of the thermal behavior of Raman peaks we consider the reduced intensity as defined from equation:

$$I_{\text{reduced}} = \frac{I_{\text{Stokes}}}{(n(\Delta\bar{\nu}, T) + 1) \cdot \nu_i \cdot (\nu_i - \Delta\bar{\nu})^3} \quad (2)$$

where $\nu_i$ is the frequency of the input laser, $\Delta\bar{\nu} = \nu_i - \nu_s$ is the relative wavenumber (or Raman shift) in $cm^{-1}$ (if $\nu_s$ is the frequency of the scattered beam) and $n(\Delta\bar{\nu},T)$ is the population factor of phonons at thermal equilibrium given by:

$$n(\Delta\bar{\nu}, T) = \frac{1}{\exp\left(\frac{h \cdot c \cdot \Delta\bar{\nu}}{k_B T}\right) - 1} \quad (3)$$

A first (and the most important) correction comes from the population factor which is known to influence largely the Raman intensity at low-wavenumber. Furthermore, since a CCD is used as detector [28, 29] the Raman intensity needs to be corrected by dividing the spectrum by this factor $(\nu_i - \Delta\bar{\nu})^3$.

The reduced intensity of the (XX) spectrum is reported in figure 4(b) for several temperatures. This plot is remarkably different from the raw data (figure 4(a)). The VLF signal shows a large change with the temperature. Nevertheless it is partly hidden by wide bands above 100 $cm^{-1}$, due to second order processes which increase in intensity with temperature, so that the numerical exploitation of VLF signal is difficult.

### 3.3. XY extinction spectra

The XY spectrum reported in figure 5(a) corresponds to the 'extinction configuration'. It is reminded that no phonon peak is detected in this spectrum in accordance with Raman selection rules. However, an intense and wide VLF signal is observed at room temperature. Its intensity diminishes rapidly on heating, then is nearly constant on approaching $T_c$ (409 K), and finally decreases abruptly at $T_c$. The VLF intensity continuously diminishes in the C phase, but remains not negligible even at high temperature (453 K).

As above, we will consider the reduced intensity [according to equation (2)], in order to properly analyze the VLF XY spectrum as a function of temperature.

By contrast of the as-measured spectrum, the reduced-intensity spectrum shown in figure 5(b), presents a remarkably different shape in the C phase, compared to the T phase. This underlines the importance of the corrections for the VLF signal. An abrupt change in the VLF signal of the spectrum (XY) occurs between 408 and 411 K, in accordance with the disappearance at $T_c$ of the first-order lines in the XX spectrum (figures 2 and 3). The VLF signal displays below $T_c$ (409 K) continuous changes in both the intensity, and the maximum position while it is much smaller and wider above $T_c$ (see the insert of figure 5(b)). Its origin in the C phase could be therefore attributed to a phonon density of states, in accordance with the centrosymmetric symmetry. In what follows we focus on the VLF signal only in the T phase.

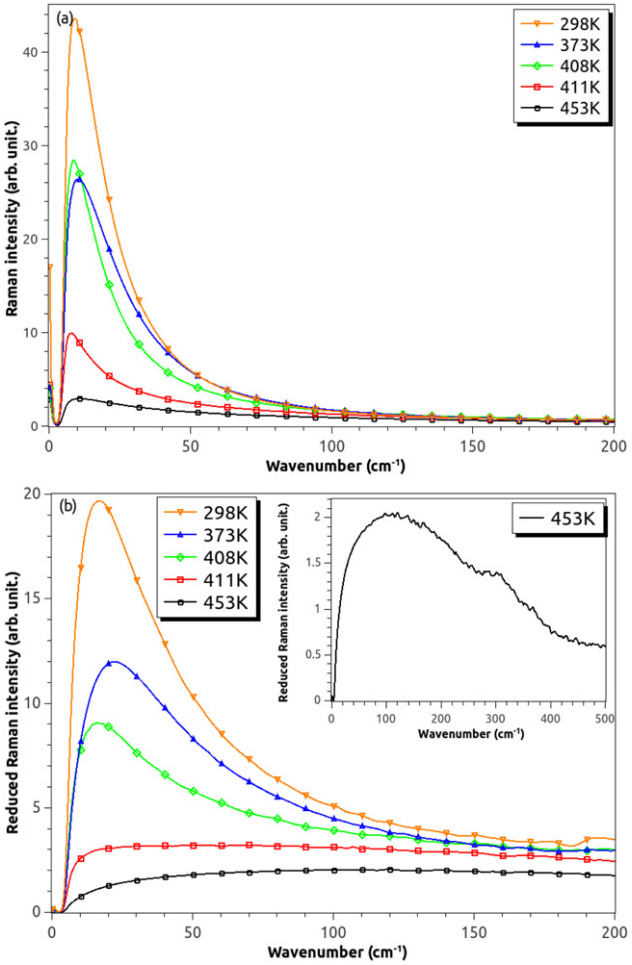


**Figure 5.** Low-frequency Z(XY)$\bar{Z}$ Raman spectrum recorded at different temperatures on single $BaTiO_3$ crystal: (a) raw data, (b) corrected data according to equation (2). Insert: spectrum measured in the C phase, within a wider wavenumber range. The shoulder around 300 $cm^{-1}$ can be attributed to FE precursor effects.

At first, we point out that the VLF signal can be unambiguously exploited in the 'extinction configuration'. In the other configurations the presence either of the soft phonon (E symmetry) within the same wavenumber range, or the second order scattering [$A_1$(TO) or $A_1$(LO)—see figure 4(b)] leads to partly or totally hide the VLF signal. It is to be underlined that the VLF signal appears in the T phase as a peak with a marked maximum, and not as an unresolved peak centered on zero (QES), as often reported in earlier investigations [18, 19].

In order to further analyze these data, we plot in figure 6(a) the integrated (reduced) intensity vs temperature. $J$ displays firstly a small increase on cooling in the C phase, then an abrupt increase at $T_c$, and then a huge and continuous growth in the T phase.

In addition, we fit the scattered (reduced) VLF response to a Debye relaxation. The results are reported as function of temperature in figure 6(b). The Debye frequency $\gamma$ shows two clear slowing down behaviors on approaching the T–C, and the T–O phase transitions. This remarkable result shows that the VLF feature detected in the 'extinction configuration' of the T phase, is without any ambiguity related to both SPT. Within

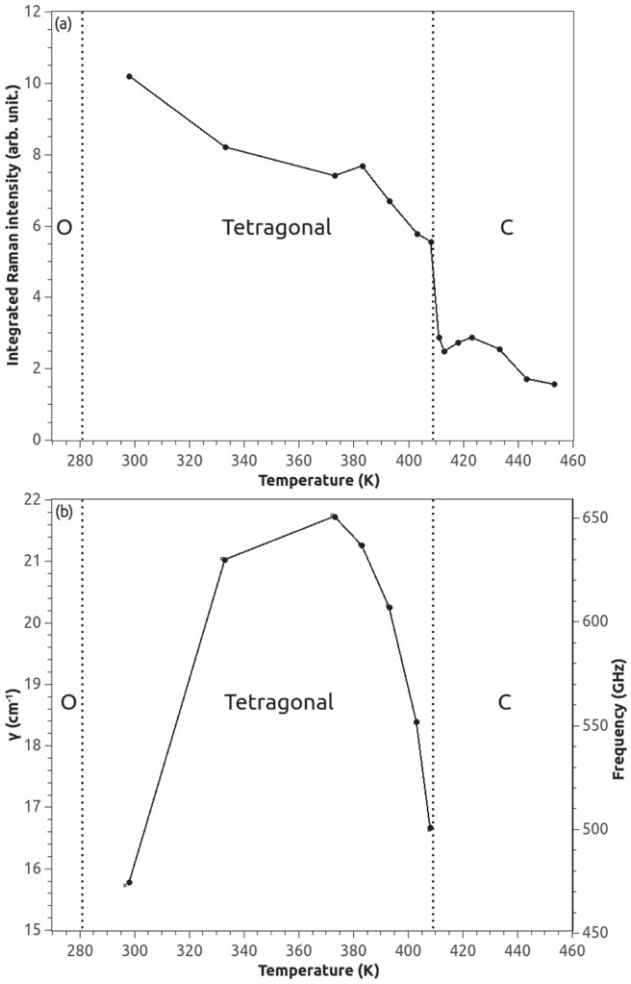


**Figure 6.** (a) Temperature dependence of the intensity $J$ integrated between 7 and 100 $cm^{-1}$ derived from data in figure 5(b). (b) Temperature dependence of the relaxation frequency.

this picture the integrated intensity of the VLF signal should correspond to the polarization fluctuation.

## 4. Discussion and conclusion

We have detected by means of ULF Raman spectroscopy a sub-THz response in tetragonal BTO, in a scattering configuration, the so-called 'extinction spectrum', which excludes the activity of any first-order phonon expected in the T phase. A pronounced peak has been highlighted in this very low-frequency range, but is clearly distinct from the soft phonon reported a long time ago. This signal appears in the T phase as a wide and asymmetric band with a maximum position below 25 $cm^{-1}$ (750 GHz). Its intensity and shape are strongly dependent on temperature and it shows a relaxation behavior with a slowing down on approaching the T–C, and the T–O SPT as well.

The sub-THz relaxation mode cannot be confused with first-order phonons, the positions of which are well known. It does not obey to the same symmetry relation rules as $E$, $B_1$ and $A_1$ phonons, and is thus consistent with hopping motion along [111] directions. As a consequence, it can be attributed to a local mode, related to Ti ion-off centering, providing an additional degree of freedom, in agreement with order–disorder model [17], and the interpretation derived from the pseudo Jahn–Teller approach [8]. The expected Raman lines in tetragonal phase arise from optical phonons due to collective vibrations of ions around their tetragonal average positions, while the additional VLF peak is related to relaxation of Ti ions which are locally displaced. This description is in agreement with the model predicted by Girshberg and Yacoby in other perovskites [30].

## ORCID iDs

Ninel Kokanyan https://orcid.org/0000-0003-2625-2671
Thomas H Kauffmann https://orcid.org/0000-0002-0621-2624

## References

[1] Lines M E and Glass A M 1977 *Principles and Applications in Ferroelectrics and Related Materials* (Oxford: Clarendon)
[2] Jona F and Shirane G 1962 *Ferroelectric Crystals* (New York: MacMillan)
[3] Luspin Y, Servoin J L and Gervais F 1980 *J. Phys. C: Solid State Phys.* **13** 3761
[4] Vogt H, Sanjurjo J A and Rossbroich G 1982 *Phys. Rev.* B **26** 5904
[5] Burns G and Dacol F H 1978 *Phys. Rev.* B **18** 5750
[6] Comès R, Lambert M and Guinier A 1968 *C R Acad. Sci. Paris* **226** 959
[7] Ravel B, Stern E A, Verdinskii R I and Kraizman V 1998 *Ferroelectrics* **206** 407
[8] Bersuker I B 2018 *Ferroelectrics* **536** 1
[9] Ko J-H, Kojima S, Koo T Y, Jung J H, Won C J and Hur N J 2008 *Appl. Phys. Lett.* **93** 102913
[10] Pasciak M, Welberry T R, Kulda J, Leoni S and Hlinka J 2018 *Phys. Rev. Lett.* **120** 167601
[11] Zhong W, Vanderbilt D and M Rabe K 1995 *Phys. Rev.* B **52** 6301
[12] Stachiotti M, Dobry A, Migoni R and Bussmann-Holder A 1993 *Phys. Rev.* B **47** 2473
[13] Hlinka J, Ostapchuk T, Nuzhnyy D, Petzelt J, Kuzel P, Kadlec C, Vanek P, Ponomareva I and Bellaiche L 2008 *Phys. Rev. Lett.* **101** 167402
[14] Muller K A, Luspin Y, Servoin J L and Gervais F 1982 *J. Physique* **43** L-537
[15] Laabidi K, Fontana M D, Maglione M, Jannot B and Muller K A 1994 *Euro. Phys. Lett.* **26** 309
[16] Petzelt J 2008 *Ferroelectrics* **375** 156
[17] Liu S, Huang L, Li J and O Brien S 2012 *J. Appl. Phys.* **112** 014108
[18] Sokoloff J P, Chase L L and Rytz D 1988 *Phys. Rev.* B **38** 597
[19] Fontana M D, Laabidi K and Jannot B 1994 *J. Phys.: Condens. Matter* **6** 8923
[20] Dougherty T P, Wiederrecht G P, Nelson K A, Garrett M H, Jensen H P and Warde C 1994 *Phys. Rev.* B **50** 8996
[21] Ponomareva I, Bellaiche L, Ostapchuk T, Hlinka J and Petzelt J 2008 *Phys. Rev.* B **77** 012102
[22] Deng H Y 2012 *Europhys. Lett.* **100** 270001
[23] Bejaoui Ouni I, Chapron D, Aroui H and Fontana M D 2016 *Appl. Phys.* A **122** 480
[24] Hoshina T, Takizawa K, Li J, Kasama T, Kakemoto H and Tsurumi T 2014 *Jpn. J. Appl. Phys.* **53** 09PD03

[25] Domenico M DJr, Wemple S H, S Porto S P and Bauman R P 1968 *Phys. Rev.* **174** 522
[26] Scalabrin A, Chaves A S, Shim D S and S Porto S P 1977 *Phys. Status. Solidi* B **79** 731
[27] Pugachev A M, Kovalevskii V I, Surovtsev N V, Kokima S, Prosandeev S A, Raevski I P and Raevskaya S I 2012 *Phys. Rev. Lett.* **108** 247601
[28] Kauffmann T H, Konanyan N and Fontana M D 2019 *J. Raman Spectrosc.* **50** 418
[29] Gallardo J J, Navas J, Zorrilla D, Alcantara R, Valor D, Fernandez-Lorenzo C and Martin-Calleja J 2016 *Appl. Spectrosc.* **70** 1128
[30] Girshberg Y and Yacoby Y 1997 *Solid State Commun.* **103** 425